第 32 卷第 9 期
2016 年 9 月

无 机 化 学 学 报
CHINESE JOURNAL OF INORGANIC CHEMISTRY

Vol.32 No.9
1611-1618

# 基于 2,4,4′-联苯三羧酸及菲咯啉的锰(Ⅱ)和镍(Ⅱ)双核配合物的合成、晶体结构及磁性质

赵素琴*,[1] 顾金忠*,[2]

([1] 青海民族大学物理与电子信息工程学院,西宁 810007)

([2] 兰州大学化学化工学院,兰州 730000)

**摘要**: 通过水热方法,用 2,4,4′-联苯三羧酸($H_3btc$)和菲咯啉(phen)分别与 $MnCl_2·4H_2O$ 和 $NiCl_2·6H_2O$ 反应,合成了 2 个具有双核结构的配合物$[Mn_2(Hbtc)_2(phen)_4]·5H_2O$ (**1**)和$[Ni_2(Hbtc)_2(phen)_4]·2H_3btc·4H_2O$ (**2**),并对其结构和磁性质进行了研究。结构分析结果表明 2 个配合物的晶体都属于三斜晶系,$P\bar{1}$ 空间群。配合物 **1** 和 **2** 均为双核结构,通过分子间的 O–H…O 氢键作用,双核的分子被进一步连接成了三维超分子框架。研究表明,双核分子中相邻金属离子间存在反铁磁相互作用。

**关键词**: 配位化合物; 锰配合物; 镍配合物; 磁性

**中图分类号**: O614.7+11; O614.81+3 **文献标识码**: A **文章编号**: 1001-4861(2016)09-1611-08

**DOI**: 10.11862/CJIC.2016.203

# Syntheses, Crystal Structures and Magnetic Properties of Mn(Ⅱ) and Ni(Ⅱ) Dinuclear Coordination Compounds Constructed from Biphenyl-2,4,4′-Tricarboxylate and Phenanthroline

ZHAO Su-Qin*,[1] GU Jin-Zhong*,[2]

([1]*College of Physics and Electronic Information Engineering, Qinghai University for Nationalities, Xining* 810007, *China*)

([2]*College of Chemistry and Chemical Engineering, Lanzhou University, Lanzhou* 730000, *China*)

**Abstract:** Two coordination compounds, namely $[Mn_2(Hbtc)_2(phen)_4]·5H_2O$ (**1**) and $[Ni_2(Hbtc)_2(phen)_4]·2H_3btc·4H_2O$ (**2**) have been constructed hydrothermally using $H_3btc$ ($H_3btc$=biphenyl-2,4,4′-tricarboxylic acid), phen (phen =phenanthroline), $MnCl_2·4H_2O$ and $NiCl_2·6H_2O$. Both compounds crystallize in the triclinic system, space group $P\bar{1}$. The compounds possess the dinuclear structures, which are further extended into the 3D supramolecular frameworks through O–H…O hydrogen bonding. Magnetic studies for compounds **1** and **2** show a weak antiferromagnetic coupling between the neighbouring metal centers, with $J$=−3.82 $cm^{-1}$ (**1**) and −2.35 $cm^{-1}$ (**2**). CCDC: 1456513, **1**; 1456514, **2**.

**Keywords:** coordination compound; Mn(Ⅱ) compound; Ni(Ⅱ) compound; magnetic properties

## 0 Introduction

In the past decades, a considerable attention was focused on the crystal engineering of metal-organic and supramolecular architectures based on different carboxylic acid building blocks and assembled by covalent bonds and various non-covalent forces (strong and weak hydrogen bonds, $\pi$-$\pi$ interactions, and

收稿日期:2016-04-16。收修改稿日期:2016-07-22。

青海省应用基础研究计划(No.2015-ZJ-738)资助项目。

*通信联系人。E-mail:qhzhsq@sina.com,gujzh@lzu.edu.cn;会员登记号:S06N5892M1004。

halogen bonding) [1-6]. This research was primarily justified by a diversity of applications of the obtained compounds that span from gas sorption, magnetism, sensing and molecular recognition to photochemistry, catalysis, and medicinal chemistry[7-15].

As is well known, many factors may seriously influence the structures of the resulting compounds, such as the ligands, kinds of metal salt, the solvent system, pH value, the metal-to-ligand ratio, reaction temperature and time, and so on[16-20]. Multicarboxylate ligands are often employed as bridging blocks to construct coordination compounds due to their versatile coordination modes and the ability to act as H-bond acceptors and donors to assemble supramolecular structures[21-26]. In order to extend our research in this field, we have selected biphenyl-2,4,4′-tricarboxylic acid ($H_3btc$) as a functional building block on account of the following considerations: (a) $H_3btc$ possesses three carboxyl groups that may be completely or partially deprotonated, depending on pH value; (b) it is a flexible ligand allowing the rotation of two phenyl rings around the C-C single bond; (c) to our knowledge, $H_3btc$ has not been adequately explored in the construction of coordination polymers[21-22].

Taking into account these factors, we herein report the syntheses, crystal structures, magnetic properties of Mn(Ⅱ) and Ni(Ⅱ) coordination compounds constructed from $Hbtc^{2-}$ and phen ligand.

## 1 Experimental

### 1.1 Reagents and physical measurements

All chemicals and solvents were of AR grade and used without further purification. Carbon, hydrogen and nitrogen were determined using an Elementar Vario EL elemental analyzer. IR spectra were recorded using KBr pellets and a Bruker EQUINOX 55 spectrometer. Thermogravimetric analysis (TGA) data were collected on a LINSEIS STA PT1600 thermal analyzer with a heating rate of 10 ℃·min$^{-1}$. Magnetic susceptibility data were collected in the 2 ~300 K temperature range with a Quantum Design SQUID Magnetometer MPMS XL-7 with a field of 0.1 T. A correction was made for the diamagnetic contribution prior to data analysis.

### 1.2 Synthesis of $[Mn_2(Hbtc)_2(phen)_4]\cdot 5H_2O$ (1)

A mixture of $MnCl_2\cdot 4H_2O$ (0.060 g, 0.3 mmol), $H_3btc$ (0.086 g, 0.3 mmol), phen (0.120 g, 0.6 mmol), NaOH (0.024 g, 0.6 mmol), and $H_2O$ (10 mL) was stirred at room temperature for 15 min, and then sealed in a 25 mL Teflon-lined stainless steel vessel, and heated at 160 ℃ for 3 days, followed by cooling to room temperature at a rate of 10 ℃·h$^{-1}$. Yellow block-shaped crystals of **1** were isolated manually, and washed with distilled water. Yield: 63% (based on Mn salt). Anal. Calcd. for $C_{78}H_{58}Mn_2N_8O_{17}$(%): C 62.91, H 3.92, N 7.52; Found (%): C 62.78, H 3.95, N 7.61. IR (KBr, cm$^{-1}$): 3 394m, 3 060m, 1 700m, 1 572s, 1 516m, 1 424s, 1 372s, 1 344m, 1 262m, 1 170w, 1 142w, 1 102 m, 1 050w, 1 004w, 912w, 850m, 774s, 734s, 682m, 660w, 630w, 550w.

### 1.3 Synthesis of $[Ni_2(Hbtc)_2(phen)_4]\cdot 2H_3btc\cdot 4H_2O$ (2)

A mixture of $NiCl_2\cdot 6H_2O$ (0.071 g, 0.3 mmol), $H_3btc$ (0.172 g, 0.6 mmol), phen (0.120 g, 0.6 mmol), NaOH (0.024 g, 0.6 mmol), and $H_2O$ (10 mL) was stirred at room temperature for 15 min, and then sealed in a 25 mL Teflon-lined stainless steel vessel, and heated at 160 ℃ for 3 days, followed by cooling to room temperature at a rate of 10 ℃·h$^{-1}$. Purple needle-shaped crystals of **2** were isolated manually, and washed with distilled water. Yield: 65% (based on Ni salt). Anal. Calcd. for $C_{108}H_{76}Ni_2N_8O_{28}$(%): C 62.24, H 3.73, N 5.46; Found (%): C 62.41, H 3.71, N 5.49. IR (KBr, cm$^{-1}$): 3 573w, 3 428w, 1 683s, 1 585s, 1 517m, 1 423s, 1 382w, 1 367w, 1 304w, 1 278w, 1 231m, 1 180 w, 1 154w, 1 086w, 1 003w, 925w, 910w, 868w, 848w, 811w, 769w, 728w, 676w, 655w, 645w, 531w.

### 1.4 Structure determination

Single-crystal data of **1** and **2** were collected at 293(2) K on a Bruker APE-Ⅱ CCD diffractometer with Mo $K\alpha$ radiation ($\lambda$=0.071 073 nm). The crystallographic data are summarized in Table 1. The selected bond lengths and angles are listed in Table 2. Hydrogen bond parameters of the compounds **1** and **2** are given in Tables 3 and 4. The structure was solved using direct methods, which yielded the positions of

all non-hydrogen atoms. These were refined first isotropically and then anisotropically. All the hydrogen atoms (except for those bound to water molecules) were placed in calculated positions with fixed isotropic thermal parameters and included in structure factor calculations at the final stage of full-matrix least-squares refinement. The hydrogen atoms of the water molecules were located by difference maps and constrained to ride on their parent O atoms. All calculations were performed using the SHELXL program[27].

CCDC: 1456513, **1**; 1456514, **2**.

**Table 1　Crystal data for compounds 1 and 2**

| Compound | 1 | 2 |
|---|---|---|
| Chemical formula | $C_{78}H_{58}Mn_2N_8O_{17}$ | $C_{108}H_{76}Ni_2N_8O_{28}$ |
| Molecular weight | 1 489.20 | 2 051.19 |
| Crystal system | Triclinic | Triclinic |
| Space group | $P\bar{1}$ | $P\bar{1}$ |
| $a$ / nm | 1.384 52(13) | 1.221 50(9) |
| $b$ / nm | 1.405 38(8) | 1.385 16(10) |
| $c$ / nm | 2.006 02(17) | 1.467 12(10) |
| $\alpha$ / (°) | 93.116(6) | 67.698(7) |
| $\beta$ / (°) | 109.822(8) | 86.452(6) |
| $\gamma$ / (°) | 103.188(6) | 77.217(6) |
| $V$ / nm$^3$ | 3.538 0(5) | 2.239 0(3) |
| $Z$ | 2 | 1 |
| $F$(000) | 1 536 | 1 060 |
| Crystal size / mm | 0.30×0.30×0.18 | 0.27×0.24×0.23 |
| $\theta$ range for data collection / (°) | 3.02~25.05 | 3.31~25.05 |
| Limiting indices | $-15 \leqslant h \leqslant 16, -16 \leqslant k \leqslant 16, -23 \leqslant l \leqslant 23$ | $-14 \leqslant h \leqslant 14, -16 \leqslant k \leqslant 16, -17 \leqslant l \leqslant 17$ |
| Reflections collected, unique ($R_{int}$) | 26 653, 12 332 (0.060 8) | 14 229, 7 939 (0.027 6) |
| $D_c$ / (g·cm$^{-3}$) | 1.398 | 1.521 |
| $\mu$ / mm$^{-1}$ | 0.434 | 0.513 |
| Data, restraints, parameters | 12 332, 114, 948 | 7 939, 1, 674 |
| Goodness-of-fit on $F^2$ | 0.963 | 1.007 |
| $R_1$, $wR_2$ [$I \geqslant 2\sigma(I)$] | 0.069 7, 0.152 7 | 0.043 9, 0.090 4 |
| $R_1$, $wR_2$ (all data) | 0.127 3, 0.186 6 | 0.053 4, 0.096 6 |
| Largest diff. peak and hole / (e·nm$^{-3}$) | 400 and −381 | 1 089 and −635 |

**Table 2　Selected bond distances (nm) and bond angles (°) for compounds 1 and 2**

| 1 | | | | | |
|---|---|---|---|---|---|
| Mn(1)–O(1) | 0.210 0(4) | Mn(1)-O(4)A | 0.210 4(3) | Mn(1)-N(1) | 0.227 4(4) |
| Mn(1)-N(2) | 0.239 7(4) | Mn(1)-N(3) | 0.232 5(4) | Mn(1)-N(4) | 0.226 7(4) |
| Mn(2)-O(9) | 0.212 5(3) | Mn(2)-O(10)B | 0.215 4(3) | Mn(2)-N(5) | 0.225 5(5) |
| Mn(2)-N(6) | 0.232 6(4) | Mn(2)-N(7) | 0.226 3(4) | Mn(2)-N(8) | 0.227 8(4) |
| | | | | | |
| O(1)-Mn(1)-O(4)A | 100.10(14) | O(1)-Mn(1)-N(4) | 112.46(15) | O(4)A-Mn(1)-N(4) | 91.69(12) |
| O(1)-Mn(1)-N(1) | 87.92(18) | O(4)A-Mn(1)-N(1) | 103.85(13) | N(4)-Mn(1)-N(1) | 151.98(16) |
| O(1)-Mn(1)-N(3) | 88.92(14) | O(4)A-Mn(1)-N(3) | 163.88(13) | N(4)-Mn(1)-N(3) | 72.44(14) |
| N(1)-Mn(1)-N(3) | 89.70(14) | O(1)-Mn(1)-N(2) | 158.33(17) | O(4)A-Mn(1)-N(2) | 90.35(13) |
| N(4)-Mn(1)-N(2) | 85.89(15) | N(1)-Mn(1)-N(2) | 71.08(17) | N(3)-Mn(1)-N(2) | 85.77(14) |
| O(9)-Mn(2)-O(10)B | 98.64(12) | O(9)-Mn(2)-N(5) | 91.39(14) | O(10)B-Mn(2)-N(5) | 90.51(16) |

Continued Table 2

| | | | | | |
|---|---|---|---|---|---|
| O(9)-Mn(2)-N(7) | 172.46(13) | O(10)B-Mn(2)-N(7) | 87.43(13) | N(5)-Mn(2)-N(7) | 93.05(15) |
| O(9)-Mn(2)-N(8) | 100.79(14) | O(10)B-Mn(2)-N(8) | 103.58(13) | N(5)-Mn(2)-N(8) | 159.62(15) |
| N(7)-Mn(2)-N(8) | 73.28(15) | O(9)-Mn(2)-N(6) | 90.56(14) | O(10)B-Mn(2)-N(6) | 161.55(17) |
| N(5)-Mn(2)-N(6) | 73.2(2) | N(7)-Mn(2)-N(6) | 84.89(14) | N(8)-Mn(2)-N(6) | 90.24(18) |
| | | **2** | | | |
| Ni(1)-O(1) | 0.208 3(2) | Ni(1)-O(2)A | 0.205 9(2) | Ni(1)-N(1) | 0.208 0(2) |
| Ni(1)-N(2) | 0.210 4(2) | Ni(1)-N(3) | 0.206 8(2) | Ni(1)-N(4) | 0.208 6(2) |
| O(2)A-Ni(1)-N(3) | 97.32(8) | O(2)A-Ni(1)-N(1) | 86.43(8) | N(3)-Ni(1)-N(1) | 172.03(9) |
| O(2)A-Ni(1)-O(1) | 88.93(7) | N(3)-Ni(1)-O(1) | 97.60(8) | N(1)-Ni(1)-O(1) | 89.47(8) |
| O(2)A-Ni(1)-N(4) | 175.73(8) | N(3)-Ni(1)-N(4) | 80.07(8) | N(1)-Ni(1)-N(4) | 95.75(8) |
| O(1)-Ni(1)-N(4) | 94.76(8) | O(2)A-Ni(1)-N(2) | 86.26(8) | N(3)-Ni(1)-N(2) | 93.22(8) |
| N(1)-Ni(1)-N(2) | 79.97(9) | O(1)-Ni(1)-N(2) | 168.64(8) | N(4)-Ni(1)-N(2) | 90.50(8) |

Symmetry codes: A: $-x$, $-y+1$, $-z+1$; B: $-x$, $-y+2$, $-z+2$ for **1**; A: $-x+1$, $-y+1$, $-z$ for **2**.

**Table 3 Hydrogen bond lengths (nm) and angles (°) of compound 1**

| D–H···A | *d*(D-H) | *d*(H···A) | *d*(D···A) | ∠DHA |
|---|---|---|---|---|
| O(6)–H(6)···O(14)C | 0.082 | 0.189 | 0.262 6 | 148.4 |
| O(8)–H(8)···O(12)D | 0.082 | 0.170 | 0.251 0 | 171.4 |
| O(13)–H(13A)···O(14) | 0.084 | 0.224 | 0.307 3 | 178.4 |
| O(13)–H(13B)···O(3) | 0.085 | 0.192 | 0.276 9 | 178.6 |
| O(14)–H(14A)···O(2)A | 0.085 | 0.202 | 0.286 9 | 178.7 |
| O(15)–H(15A)···O(3) | 0.085 | 0.216 | 0.283 9 | 136.6 |
| O(16)–H(16B)···O(7)E | 0.085 | 0.216 | 0.300 7 | 179.7 |
| O(17)–H(17A)···O(13) | 0.098 | 0.213 | 0.298 5 | 144.8 |

Symmetry codes: A: $-x$, $-y+1$, $-z+1$; B: $-x$, $-y+2$, $-z+2$; C: $x-1$, $y$, $z$; D: $x+1$, $y$, $z$; E: $x$, $y-1$, $z$.

**Table 4 Hydrogen bond lengths (nm) and angles (°) of compound 2**

| D–H···A | *d*(D-H) | *d*(H···A) | *d*(D···A) | ∠DHA |
|---|---|---|---|---|
| O(3)–H(1)···O(6)A | 0.082 | 0.179 | 0.260 6 | 172.2 |
| O(7)–H(2)···O(5)B | 0.082 | 0.177 | 0.258 3 | 170.4 |
| O(10)–H(4)···O(12)C | 0.082 | 0.180 | 0.261 8 | 172.8 |
| O(11)–H(5)···O(9)A | 0.084 | 0.177 | 0.261 3 | 175.0 |
| O(13)–H(1W)···O(6)B | 0.092 | 0.198 | 0.290 4 | 174.0 |
| O(13)–H(2W)···O(14)E | 0.073 | 0.212 | 0.283 0 | 166.0 |
| O(14)–H(3W)···O(13)D | 0.085 | 0.197 | 0.282 2 | 179.7 |
| O(14)–H(4W)···O(8)B | 0.085 | 0.213 | 0.298 3 | 179.7 |

Symmetry codes: A: $x$, $y-1$, $z$; B: $-x+1$, $-y+1$, $-z+1$; C: $x$, $y+1$, $z$; D: $-x+2$, $-y+1$, $-z+1$; E: $x$, $y-1$, $z+1$.

## 2 Results and discussion

### 2.1 Description of the structures

#### 2.1.1 $[Mn_2(Hbtc)_2(phen)_4]\cdot 5H_2O$ (**1**)

The X-ray crystallography analysis reveals that the compound **1** crystallizes in the triclinic system space group $P\bar{1}$. The asymmetric unit of compound **1** contains two crystallographically unique Mn(Ⅱ) atoms, two $Hbtc^{2-}$ ligands, four phen moieties, and five lattice water molecules. The partial deprotonation of $H_3btc$ to give $Hbtc^{2-}$ is also confirmed by the IR spectral data of **1**, since a band -COOH band at 1 700 $cm^{-1}$ was

observed (Experimental Section). As depicted in Fig.1, both Mn1 and Mn2 atoms are six-coordinated by two carboxylate O atoms of two independent $Hbtc^{2-}$ ligands and four N atoms of two phen moieties, forming a distorted octahedral geometry. The Mn-O (0.210 0(4)~0.215 4(3) nm) and Mn-N (0.225 5(5)~0.239 7(4) nm) bond lengths are in good agreement with those distances observed in some other Mn(Ⅱ) compounds[17,21,23-24]. As shown in Fig.2, two crystallographically equal Mn1 centers are bridged by 2- and 4-carboxylate groups of two different $Hbtc^{2-}$ blocks, giving rise to a dinuclear unit Ⅰ with a Mn⋯Mn separation of 0.810 0(4) nm. Simultaneously, 2-carboxylate groups of two different $Hbtc^{2-}$ blocks bridge two crystallographically equal Mn2 centers to form another dinuclear unit Ⅱ with a Mn⋯Mn separation of 0.427 9(4) nm. Obviously, dinuclear $Mn_2$ units Ⅰ and Ⅱ are isomers. The dihedral angles of two benzene rings in the $Hbtc^{2-}$ blocks are 45.04° and 63.97°, respectively. These dinuclear $Mn_2$ units are further extended into the 3D supramolecular frameworks through O–H⋯O hydrogen bonding (Fig.3 and Table 3).

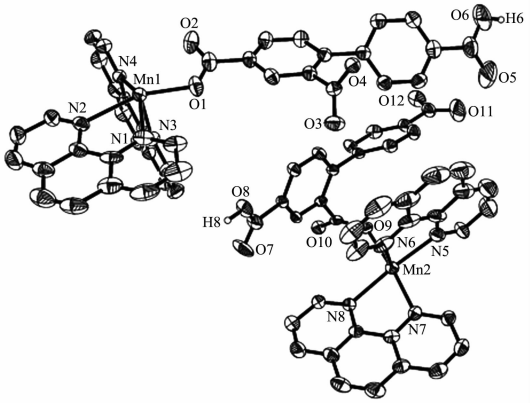


H atoms were omitted for clarity except those of COOH groups

Fig.1　Drawing of the asymmetric unit of compound **1** with 30% probability thermal ellipsoids

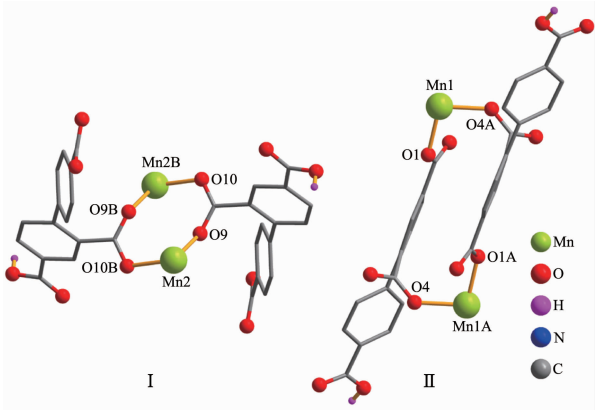


Phen ligands were omitted for clarity; Symmetry codes: A: $-x$, $-y+1$, $-z+1$; B: $-x$, $-y+2$, $-z+2$

Fig.2　Dinuclear $Mn_2$ units Ⅰ and Ⅱ in compound **1**

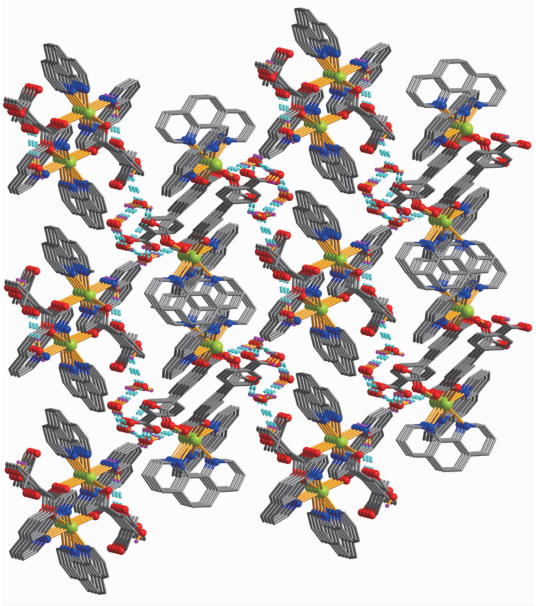

Dashed lines represent the H-bond

Fig.3　Perspective view of 3D supramolecular structure in the *bc* plane

### 2.1.2　$[Ni_2(Hbtc)_2(phen)_4]\cdot 2H_3btc\cdot 4H_2O$ (**2**)

In complex **2**, the asymmetric unit consists of one Ni(Ⅱ) atom, one $Hbtc^{2-}$ block, two lattice water molecules, and a molecule of co-crystallized $H_3btc$ (Fig.4). The six-coordinate Ni1 center is bound by four N atoms from two phen ligands and two carboxylate O atoms from two different $Hbtc^{2-}$ blocks, thus forming

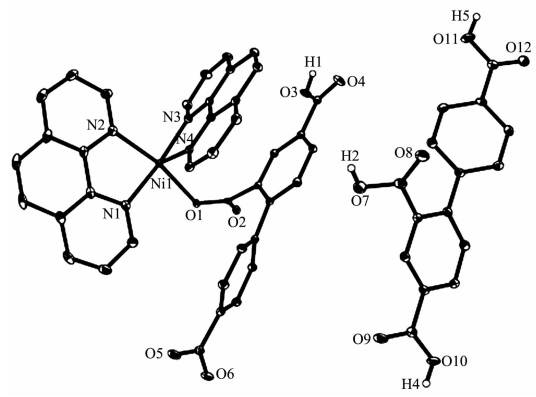


H atoms were omitted for clarity except those of COOH groups

Fig.4　Drawing of the asymmetric unit of compound **2** with 30% probability thermal ellipsoids

an octahedral $\{NiN_4O_2\}$ geometry. The Ni-O bonds are in the range of 0.205 9(2)~0.208 3(2) nm, while the Ni-N distances vary from 0.206 8(2)~0.210 4(2) nm; all these distances are comparable to those found in the reported Ni(Ⅱ) compounds[21-22,26,28]. In **2**, two crystallographically equal Ni1 centers are bridged by 2-carboxylate groups of two different $Hbtc^{2-}$ blocks, giving rise to a dinuclear $Ni_2$ unit with a Ni … Ni separation of 0.479 8(4) nm (Fig.5). Obviously, the $Ni_2$ dinuclear unit and the $Mn_2$ dinuclear unit Ⅱ in **1** are isostructural. The dihedral angle of two benzene rings in the $Hbtc^{2-}$ and $H_3btc$ are 45.80° and 35.07°, respectively. The discrete $Ni_2$ units and free $H_3btc$ molecules are interlinked by the strong O–H…O hydrogen bonds to form a 3D supramolecular framework (Fig.6, Table 4).

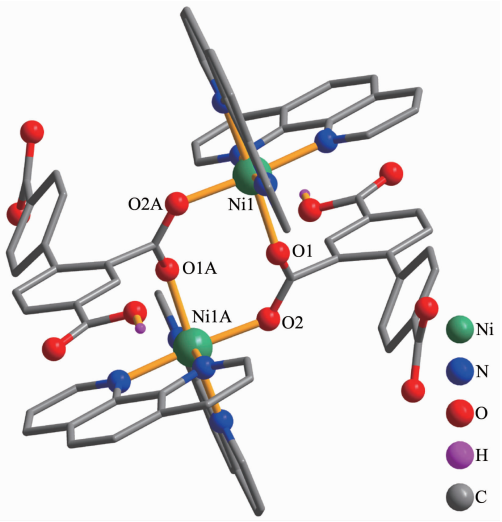


H atoms were omitted for clarity except those of COOH groups; Symmetry codes: A: $-x+1, -y+1, -z$

Fig.5 Dinuclear $Ni_2$ unit in compound **2**

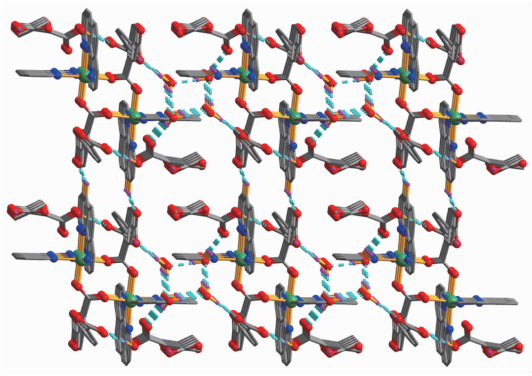

Dashed lines represent the H-bond

Fig.6 Perspective view of 3D supramolecular structure in the *ac* plane

## 2.2 TGA analysis

The thermal stability of **1** and **2** was investigated under nitrogen atmosphere by thermogravimetric analysis (TGA); the obtained plots are shown in Fig.7. Compound **1** loses its five lattice water molecules (Found 5.85%; Calcd. 6.04%) in the 28~116 ℃ range, followed by the decomposition starting at 205 ℃. For **2**, there are two distinct thermal effects in the 98~238 ℃ range that correspond to the removal of four free $H_2O$ molecules (Found 3.45%; Calcd. 3.51%) and two co-crystallization $H_3btc$ molecules (Found 32.1%; Calcd. 31.5%), followed by the concomitant decomposition.

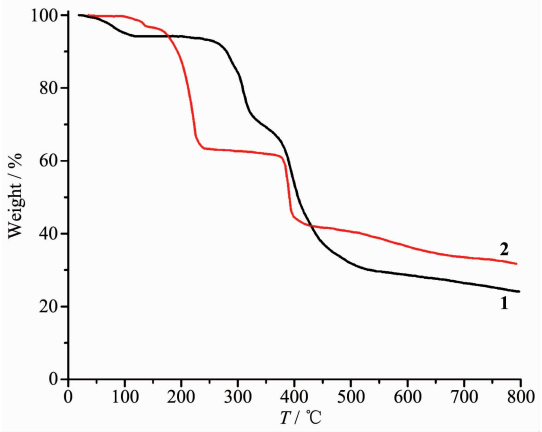


Fig.7 TGA curves of compounds **1** and **2**

## 2.3 Magnetic properties

Variable-temperature magnetic susceptibility studies were carried out on powder samples of **1** and **2** in the 2~300 K temperature range. For **1**, the $\chi_M T$ value at 300 K is 8.81 $cm^3 \cdot mol^{-1} \cdot K$, which is close to the value of 8.76 $cm^3 \cdot mol^{-1} \cdot K$ expected for two magnetically isolated high-spin Mn(Ⅱ) centers ($S_{Mn}$=5/2, $g$=2.0). Upon cooling, the $\chi_M T$ value drops down very slowly from 8.81 $cm^3 \cdot mol^{-1} \cdot K$ at 300 K to 8.38 $cm^3 \cdot mol^{-1} \cdot K$ at 98 K and then decreases steeply to 1.50 $cm^3 \cdot mol^{-1} \cdot K$ at 2 K (Fig.8). The $\chi_M^{-1}$ vs $T$ plot for **1** in the 2~300 K interval obeys the Curie-Weiss law with a Weiss constant $\theta$ of −10.40 K and a Curie constant $C$ of 9.10 $cm^3 \cdot mol^{-1} \cdot K$. The negative value of $\theta$ and the decrease of the $\chi_M T$ should be attributed to the overall antiferromagnetic coupling between the Mn(Ⅱ) centers within the $Mn_2$ unit. We tried to fit the magnetic data of **1** using the following expression[29-30] for the dinuclear Mn(Ⅱ) unit:

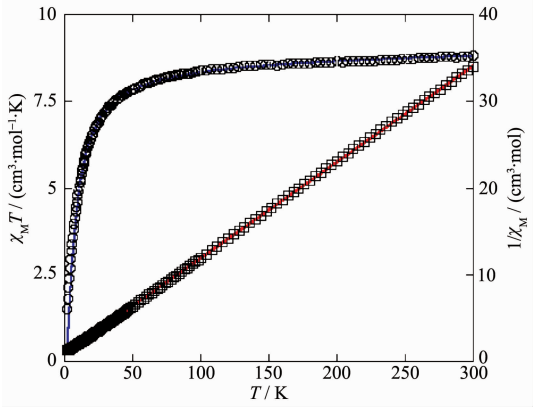


Curve represents the best fit to the equations in the text; Straight line shows the Curie-Weiss fitting

Fig.8　Temperature dependence of $\chi_M T$ (○) and $1/\chi_M$ (□) vs $T$ for compound **1**

$$H=-JS_1S_2 \quad (1)$$

$$\chi_M=2\frac{Ng^2\beta^2}{KT}\frac{A}{B} \quad (2)$$

$$A=\exp[2J/(KT)]+5\exp[6J/(KT)]+14\exp[12J/(KT)]+30\exp[20J/(KT)]+55\exp[30J/(KT)] \quad (3)$$

$$B=1+3\exp[2J/(KT)]+5\exp[6J/(KT)]+7\exp[12J/(KT)]+9\exp[20J/(KT)]+11\exp[30J/(KT)] \quad (4)$$

Least-squares analysis of magnetic susceptibility data led to $J$=−3.82 cm$^{-1}$, $g$=2.00 and $R$=3.46×10$^{-5}$. These values confirm the presence of antiferromagnetic interaction between the Mn(Ⅱ) ions within the dinuclear units. Because of the long separation within the dinuclear $Mn_2$ unit Ⅰ (0.810 0(4) nm), the negative value of $J$ should be attributed to the antiferromagnetic coupling between the Mn(Ⅱ) atoms within the $Mn_2$ unit Ⅱ.

For **2**, the $\chi_M T$ value at 300 K is 2.18 cm$^3$·mol$^{-1}$·K, which is higher than the spin only value of 2.00 cm$^3$·mol$^{-1}$·K for two magnetically isolated Ni(Ⅱ) center ($S_{Ni}$=1, $g$=2.0). Upon cooling, the $\chi_M T$ value drops down very slowly from 2.18 cm$^3$·mol$^{-1}$·K at 300 K to 2.11 cm$^3$·mol$^{-1}$·K at 96 K, and then decreases steeply to 0.73 cm$^3$·mol$^{-1}$·K at 2 K (Fig.9). In the 2~300 K interval, the $\chi_M^{-1}$ vs $T$ plot for **2** obeys the Curie-Weiss law with a Weiss constant $\theta$ of −6.58 K and a Curie constant $C$ of 2.11 cm$^3$·mol$^{-1}$·K, suggesting a weak antiferromagnetic interaction between the Ni(Ⅱ) ions.

We tried to fit the magnetic data of **2** using the following expression[31] for a dinuclear Ni(Ⅱ) unit:

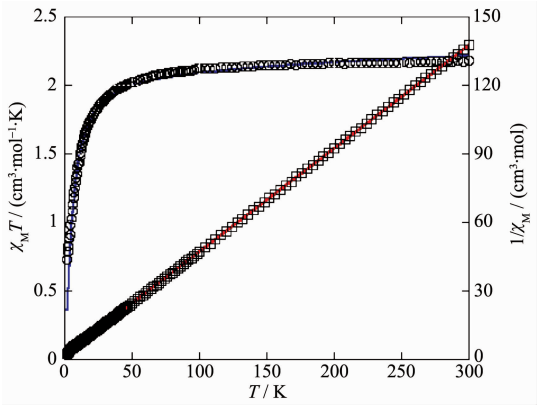


Curve represents the best fit to the equations in the text; Straight line shows the Curie-Weiss fitting

Fig.9　Temperature dependence of $\chi_M T$ (○) and $1/\chi_M$ (□) vs $T$ for compound **2**

$$H=-JS_1S_2$$

$$\chi_M=\frac{N\beta^2g^2}{3k(T-\theta)}\frac{\sum S'(S'+1)(2S'+1)e^{-ES'/(kT)}}{\sum(2S'+1)e^{-ES'/(kT)}}$$

$$\chi_M=\chi_{M'}(1-\rho)+\frac{4S(S+1)N\beta^2g^2\rho}{3kT}+\mathrm{TIP}$$

where $\rho$ is a paramagnetic impurity fraction and TIP is temperature independent paramagnetism. Using this model, the susceptibility for **2** above 2.0 K was simulated, leading to the values of $J$=−2.35 cm$^{-1}$, $g$=2.09, $\rho$=0.011, and TIP=4.56×10$^{-6}$ cm$^3$·mol$^{-1}$, with the agreement factor $R$=7.57×10$^{-4}$ ($R=\sum(T_{obs}-T_{calc})^2/\sum T_{obs}^2$). The negative $J$ parameter confirms that a weak antiferromagnetic exchange coupling exists between the adjacent Ni(Ⅱ) centers, which is in agreement with a negative $\theta$ value. In compounds **1** and **2**, there is one type of the magnetic exchange pathway within the dinuclear $Mn_2$ and $Ni_2$ units, namely via double $\mu_2$-$\eta^1$:$\eta^1$-carboxylate (*syn-syn*) bridges (Fig.1 and 5).

## 3　Conclusions

In summary, two new compounds, namely $[Mn_2(Hbtc)_2(phen)_4]\cdot 5H_2O$ (**1**) and $[Ni_2(Hbtc)_2(phen)_4]\cdot 2(H_3btc)\cdot 4H_2O$ (**2**) have been synthesized under hydrothermal conditions. Both compounds feature the dinuclear structures, which are further extended into the 3D supramolecular frameworks through O−H⋯O hydrogen bonding. Magnetic studies for two compounds show a weak antiferromagnetic coupling

between the adjacent metal centers.

## References:


[1] Seoane B, Castellanos S, Dikhtiarenko A, et al. *Coord. Chem. Rev.*, **2016**,**307**:147-187

[2] Zheng X D, Lu T B. *CrystEngComm*, **2010**,**12**:324-336

[3] Almáši M, Zeleňák V, Zukal A, et al. *Dalton Trans.*, **2016**, **45**:1233-1242

[4] Reger D L, Leitner A P, Smith M D. *Cryst. Growth Des.*, **2016**,**16**:527-536

[5] Yin Z, Zhou Y L, Zeng M H, et al. *Dalton Trans.*, **2015**,**44**: 5258-5275

[6] Bertani R, Sgarbossa P, Venzo A, et al. *Coord. Chem. Rev.*, **2010**,**254**:677-695

[7] Kreno L E, Leong K, Farha O K, et al. *Chem. Rev.*, **2012**,**112**: 1105-1125

[8] Horike S, Umeyama D, Kitagawa S. *Acc. Chem. Res.*, **2013**, **46**:2376-2384

[9] Yan Y, Yang S H, Blake A J, et al. *Acc. Chem. Res.*, **2014**, **47**:296-307

[10]DeCoste J B, Peterson G W. *Chem. Rev.*, **2014**,**114**:5695-5727

[11]Chughtai A H, Ahmad N, Younus H A, et al. *Chem. Soc. Rev.*, **2015**,**44**:6804-6849

[12]Li X J, Chen X Y, Jiang F L, et al. *Chem. Commun.*, **2016**, **52**:2277-2280

[13]Zheng H Q, Zhang Y N, Liu L F, et al. *J. Am. Chem. Soc.*, **2016**,**138**:962-968

[14]Li C, Sun M H, Xu L, et al. *CrystEngComm*, **2016**,**18**:596-600

[15]Zeng M H, Yin Z, Tan Y X, et al. *J. Am. Chem. Soc.*, **2014**, **136**:4680-4688

[16]Li C P, Wu J M, Du M. *Chem. Eur. J.*, **2012**,**18**:12437-12445

[17]Gu J Z, Gao Z Q, Tang Y. *Cryst. Growth Des.*, **2012**,**12**:3312-3323

[18]Gu J Z, Wu J, Lv D Y, et al. *Dalton Trans.*, **2013**,**42**:4822-4830

[19]Chen L, Gou S H, Wang J Q. *J. Mol. Struct.*, **2011**,**991**:149-157

[20]Lu W G, Jiang L, Lu T B. *Cryst. Growth Des.*, **2010**,**10**:4310-4318

[21]Gu J Z, Kirillov A M, Wu J, et al. *CrystEngComm*, **2013**,**15**: 10287-10303

[22]Shao Y L, Cui Y H, Gu J Z, et al. *CrystEngComm*, **2013**,**18**: 765-778

[23]Shao Y L, Cui Y H, Gu J Z, et al. *RSC Adv.*, **2015**,**5**:87484-87495

[24]Zhao Y, Chang X H, Liu G Z, et al. *Cryst. Growth Des.*, **2015**, **15**:966-974

[25]Wang Y S, Zhou Z M. *J. Solid State Chem.*, **2015**,**228**:117-123

[26]LÜ Dong-Yu(吕东煜), GAO Zhu-Qing(高竹青), GU Jin-Zhong(顾金忠), et al. *Chinese J. Inorg. Chem.*(无机化学学报), **2011**,**27**(11):2318-2322

[27]Sheldrick G M. *SHELXL NT, Version* 5.1, *Program for Solution and Refinement of Crystal Structures*, University of Göttingen, Germany, **1997**.

[28]GAO Peng(高鹏), BING Ying-Ying(邴颖颖), ZHANG Ling-Ling(张玲玲), et al. *Chinese J. Inorg. Chem.*(无机化学学报), **2015**,**31**(11):2236-2242

[29]Ma L F, Wang L Y, Du M. *CrystEngComm*, **2009**,**11**:2593-2596

[30]Carlin R L. *Magnetochemsitry*. Berlin: Springer, **1986**.

[31]Thompson L K, Niel V, Grove H. *Polyhedron*, **2004**,**23**:1175-1184